Universities of Leeds, Sheffield and York
http://eprints.whiterose.ac.uk/

Dosimetric verification of the Anisotropic Analytical Algorithm for radiotherapy treatment planning

Christopher M. Bragg[a,b][*] and John Conway[a]

[a]Department of Radiotherapy Physics, Weston Park Hospital, Sheffield Teaching Hospitals NHS Foundation Trust, S10 2SJ, UK

[b]Department of Medical Physics, Faculty of Medicine, University of Sheffield, Sheffield, S10 2JF, UK

Abstract

Background and purpose: To investigate the accuracy of photon dose calculations performed by the Anisotropic Analytical Algorithm, in homogeneous and inhomogeneous media and in simulated treatment plans.

Materials and methods: Predicted dose distributions were compared with ionisation chamber and film measurements for a series of increasingly complex situations. Initially, simple and complex fields in a homogeneous medium were studied. The effect of inhomogeneities was investigated using a range of phantoms constructed of water, bone and lung substitute materials. Simulated treatment plans were then produced using a semi-anthropomorphic phantom and the delivered doses compared to the doses predicted by the Anisotropic Analytical Algorithm.

Results: In a homogeneous medium, agreement was found to be within 2% dose or 2mm dta in most instances. In the presence of heterogeneities, agreement was generally to within 2.5%. The simulated treatment plan measurements agreed to within 2.5% or 2mm.

Conclusions: The accuracy of the algorithm was found to be satisfactory at 6MV and 10MV both in homogeneous and inhomogeneous situations and in the simulated treatment plans. The algorithm was more accurate than the Pencil Beam Convolution model, particularly in the presence of low density heterogeneities.

Introduction

A high degree of accuracy in the delivery of dose is a long-established requirement of radiotherapy treatments [4,12]. In order to achieve such accuracy, the uncertainties in all stages of the radiotherapy process, from simulation and planning to the treatment delivery, must be reduced as far as possible [17]. Crucial to this is a need for knowledge and understanding of the magnitude of the potential errors associated with each stage of the process.

The introduction of increasingly complex treatment techniques and with it the possibility for delivering higher doses in radiotherapy treatments has reinforced the requirement for accuracy in dose calculation algorithms. Historically, one of the most serious weaknesses in treatment planning systems has been their ability to accurately predict doses in the presence of inhomogeneities, particularly through poor consideration of electron transport [7,22]. Inaccuracies in dose calculation result in systematic errors in radiotherapy treatments and so are of particular importance [13].

The Anisotropic Analytical Algorithm (AAA) is the most recent photon dose calculation algorithm to be implemented in the Eclipse treatment planning system (Varian Medical Systems, Palo Alto, CA, USA). Developed by Ulmer *et al.* [24,25], it is a convolution superposition model that utilises pre-calculated treatment-unit specific parameters together with beam data measured on the end user's linear accelerators to model the clinical treatment beams. The inhomogeneity correction is implemented through the scaling of photon and electron scatter kernels anisotropically, according to the electron density distribution of the treated medium [26].

In this study, we aim to verify the accuracy of the AAA in a range of situations. The algorithm's performance in homogeneous media is investigated through comparison with measurements in water, initially for simple beam geometries and subsequently for more complex situations. Comparisons in a series of solid phantoms enable evaluation of the algorithm's ability to accurately predict the dose in inhomogeneous media. Simulated treatment plans are then applied to a semi-anthropomorphic phantom in order to test the overall dosimetric performance of the algorithm in clinically realistic situations.

Materials and Methods

Equipment Used

Initial beam measurements used for the configuration of the AAA were made using a 0.04 Wellhöfer CC04 ionisation chamber (Wellhöfer Dosimetrie, Schwarzenbruck, Germany). The configuration process required only open, asymmetric beams measurements to be entered; no measurements with the Enhanced Dynamic Wedge (EDW) or MLC were needed, other than the average MLC transmission. The configuration parameters used for dose calculations were not manually altered following the configuration, with the exception of the EDW parameters, which were adjusted to minimise the mean difference between the calculated and measured wedge factors across all wedge angles and field sizes.

Measurements were performed on a Varian 2100C/D linear accelerator using 6MV and 10MV X-ray beams. Beam profile and depth dose measurements in water were made using the Wellhöfer Blue Phantom and WP700 software and a 0.04cc Wellhöfer CC04 ionisation chamber. Measurements in inhomogeneous situations were made in solid phantoms constructed of combinations of Plastic Water^{TM} (CIRS, Inc., Norfolk, VA), bone-equivalent blocks of relative electron density 1.71 (St. Bartholomew's, London, UK), cork as a lung substitute and Styrofoam to test the algorithm in an extreme situation of low density. The relative electron densities of the cork and the Styrofoam were 0.24 and 0.05 respectively. Measurements in solid phantoms were made using a PTW model 31016 (0.016cc) pinpoint chamber (PTW-Freiburg, Freiburg, Germany), a 0.6cc Farmer chamber (Thermo Electron Corporation, Waltham, MA) and films from a single batch of Kodak XOMAT-V. The films were scanned using a VIDAR VXR-12 film scanner (VIDAR Systems Corporation, Herndon, VA), using 75 dots per inch resolution. The CIRS Thorax phantom was used for the measurement of simulated treatment plans.

All planning work was done using parameters representative of those used clinically at Weston Park Hospital. All solid phantoms were CT scanned with a slice spacing of either 5mm or 2.5mm. Dose calculations were performed using version 7.5.18 of the Eclipse Dose Calculation Server, using a 2.5mm calculation grid. Calculations performed with the system's older Pencil Beam Convolution algorithm [23] for comparison used the same grid size and an Equivalent Tissue-Air Ratio (ETAR) inhomogeneity correction, in line with current practice at our institution.

Experimental geometries

Simple, homogeneous, geometries were tested using set-ups S1-S5 in Table 1. Percentage depth dose (PDD) curves and both inplane and crossplane profiles were measured through the field central axis for square and rectangular fields. Profiles for MLC-defined fields were measured such that the plane of measurement was beneath the full thickness of the leaves. (For profiles perpendicular to the direction of leaf motion, closed leaf pairs were offset from the field axis by 1cm so that the profiles were not measured beneath the rounded leaf ends. For profiles parallel to the direction of leaf motion, the chamber was offset by 2.5mm – half the leaf width – from the field axis.) EDW field wedge factors were calculated as the ratio of the central axis dose at a depth of 5cm from the open field to the dose at the same point from the wedged field and EDW profiles were measured with film.

Except where indicated otherwise, all PDD curves and profiles were normalised independently to the depth of dose maximum and the centre of the field respectively. Calculated and measured profiles were compared at 0.25mm intervals. PDD curves were compared at depth intervals of 0.25mm. Differences between the measured and calculated curves were calculated with respect to the measured central axis dose maximum for PDD curves and to the field central axis dose for profiles:

$$\text{Dose difference (profiles)} = 100 \times \left(\frac{D_{calc} - D_{meas}}{D_{meas,CAX}} \right) \%$$

$$\text{Dose difference (PDDs)} = 100 \times \left(\frac{D_{calc} - D_{meas}}{D_{max,meas}} \right) \%$$

The performance of the algorithm in more complex situations, C1-C5 in Table 1, was then tested. For the asymmetric fields, PDD curves were measured at the centre of the fields and profiles were measured in the direction of the asymmetry. The effect of oblique incidence was tested by measuring vertical PDD curves and horizontal profiles. Calculations with a lack of backscatter material were compared to solid water depth dose measurements using the geometry shown in Figure 1 (a), made with the couch top removed using the Farmer chamber. Point dose measurements, corrected for output, were made at 5mm intervals in the deepest 5cm of the phantom. The effect of missing side-scatter was investigated using the pinpoint chamber by measuring the dose at a point with a varying thickness, x, (from 1cm to 11cm) of side scatter material using tangential fields, as shown in Figure 1 (b). The set-ups for these measurements are summarised in Table 1. The measurements and calculated doses were normalised to the respective doses in the full scatter situation for the missing scatter investigations.

The third group of measurements investigated the accuracy of the algorithm in the presence of inhomogeneities. Firstly, point dose measurements were made at 6MV and 10MV beneath five combinations of inhomogeneities and compared to the predicted doses from the AAA. All measurements were made using an SSD of 90cm with a Farmer chamber positioned at the isocentre, 10cm below the surface. The combinations of materials above and below the chamber, from the surface down, are listed in set-ups I1-I5 in Table 1. All measurements in set-ups I1-I5 were made using a 10x10cm field.

The effect of inhomogeneities on dose profiles was investigated by positioning film at a depth of 10cm in a phantom constructed of Plastic Water^{TM} and cork, as in Table 1 (set-up I6). The ability of the AAA to model the effect of layers of inhomogeneity on depth doses was investigated using a phantom constructed of Plastic Water^{TM} and Styrofoam – set-up I7 in Table 1. Depth dose measurements were made through the phantom with a Farmer chamber and compared to the PDD curves calculated by Eclipse using both the AAA and the Pencil Beam Convolution (PBC) model with ETAR inhomogeneity correction.

Finally, simulated treatment plans were produced to test the performance of the AAA in the presence of clinically realistic inhomogeneous situations. The plans were produced using CT data for the CIRS Thorax Phantom (CIRS Inc., Norfolk, VA, USA). This semi-anthropomorphic phantom includes lung (relative electron density 0.207) and spinal column (relative electron density 1.506) inhomogeneities and ten removable inserts allow the use of the pinpoint ionisation chamber for dose measurements in various locations. A three-field lung plan was produced for a centrally located tumour and a simple parallel pair plan was also created. The plans were calculated using the AAA, as well as the Pencil Beam Convolution algorithm with ETAR inhomogeneity correction for comparison. The plans were delivered to the phantom and point dose measurements were made using the pinpoint chamber in several of the measurement locations. Differences between the measured and calculated doses were expressed as a percentage of the measured dose.

Results

Simple Geometries

For square and rectangular fields at both 6MV and 10MV, the calculated depth doses beyond d_{max} agreed with measurements to within 1.5% at all points. In the square fields' build-up region, a maximum distance to agreement of 1.1mm was found for 6MV and 1.6mm for 10 MV. For the rectangular fields, all isodoses agreed to within 2mm. The mean deviations from the measured depth doses tended to increase with field size but were all smaller than 0.5%. Over all field sizes, there was a mean difference (AAA – measurement) of 0.2 ± 0.2% (1 s.d.) beyond d_{max} and 0.2 ± 2.1% (with a mean distance to agreement of 0.3 ± 0.7mm) superficial to d_{max}.

The profiles generally showed excellent agreement between calculated and measured doses. For the purposes of this work, the high dose gradient region was defined as an area in which the dose gradient exceeded 3% per mm. The low dose, low dose gradient region was defined as a region of low dose gradient in which the dose was also below 7% of the central axis dose [28]. Regions in which the dose was above 90% of the central axis dose and the dose gradient was no higher than 3% per mm were considered to be high dose, low dose gradient regions.

The maximum discrepancy in the low dose, low dose gradient region was 2% with the exception of the 30x30cm 10MV field, for which the AAA underestimated the dose by approximately 2.5%, while the maximum isodose shift in the high dose gradient regions was 1.8mm. (There was a general tendency in all profiles for the AAA to underestimate the dose outside the field.) The maximum disagreement in the high dose, low dose gradient region was generally better than 2.0% with a few exceptions; some fields show higher underestimates in the shoulder region just above the high dose gradient – typically around the 90% to 100% isodoses. The largest such difference was an underestimate of 6.7%, found in the 40x40cm 10MV field. However, in each of these cases, the predicted and measured curves were separated by no more than 2.5mm.

The fields at 90cm and 120cm SSD showed similar levels of agreement to the square fields at 100cm SSD. All discrepancies in the PDD curves below d_{max} were smaller than 1.3% and the maximum distance to agreement in the build-up region was 2.0mm. Beyond d_{max}, the maximum discrepancy between calculated and measured PDDs was 1.3%. The maximum isodose shift in the high dose gradient region of the profiles was 0.7mm at 90cm SSD and 1.3mm at 120cm. In the low dose, low dose gradient region, calculated and measured doses agreed to within 1.6%. Between the high dose

gradient regions, maximum dose differences of 1.6% and 2.8% were seen at 90cm SSD and 120cm SSD respectively, but all points were within 2mm distance to agreement.

The calculated PDDs for MLC-defined fields also showed excellent agreement with measurement; the maximum difference in the build-up region was 1.8mm and beyond d_{max}, all doses agreed to within 1.3%. The profiles exhibited the same trends as for the collimator-defined fields. In the regions of high dose gradient, the maximum distance to agreement was 1.8mm. In the low dose, low dose gradient regions, the maximum dose discrepancies were 1.6% at the lower energy and 2.1% at 10 MV. In the high dose region, all but four points agreed to within 2% or 2mm.

The final simple geometries studied were square fields with enhanced dynamic wedges. For all field sizes, the predicted wedge factor agreed less well with the measured factor as the wedge angle increased. It was decided to configure the wedges such that the maximum error in the wedge factors was minimised. Therefore, for smaller wedge angles the predicted value was an underestimate of the true wedge factor while for the larger angles, it was an overestimate. As a result, the mean error in the wedge factors for any field size was small, not exceeding 0.5%. Two calculated factors (the 60° wedge for a 5x5 cm field at each energy) varied from the measured values by more than 2%. Across all field sizes and wedge angles, the mean discrepancy was 0.0% ±1.2% (1 s.d.).

The EDW profiles were measured with film and the calibration of the film verified with point dose measurements. Excellent agreement was seen between the measured and calculated doses, as shown by the example for the 6MV 20x20cm 60° field in Figure 2. Agreement within the high dose gradient regions was to within 2mm, while in the wedged part of the field, the maximum discrepancy was 1.9%. The AAA slightly overestimated the gradient of the wedged part of the field. Agreement was similar for the 60° wedge at 10MV and the 30° wedges.

Complex Geometries

The calculated half-beam blocked fields' profiles all agreed with measurement to within 2% or 2mm in most areas. There was a tendency to consistently underestimate the dose in the high dose region away from the central axis by approximately 1%. There was also a larger underestimate of the dose in the less steep low dose part of the penumbra of the jaw aligned with the central axis than was seen for

open fields. This effect was exaggerated in the penumbra of the jaw that was moved across the central axis, although the distance to agreement remained within 3mm.

The disagreement in the case of the half-beam blocked EDW field, shown in Figure 2, was slightly greater than that for the symmetric EDW fields, with a maximum dose discrepancy of approximately 5%, close to the peak of the profile. Again, the distances to agreement in the steep dose gradients were less than 2mm.

The oblique fields' PDDs in the vertical plane through the isocentre, shown in Figure 3, showed generally good agreement, the poorest comparison being in the penumbra region. For the field incident at 20°, the algorithm underestimated the dose by more than 3% in the region between 15% and 35% of the isocentre dose, the largest discrepancy being 5.7% and the highest distance to agreement of any isodose being 6.3mm. The 30° field showed better agreement; although there were differences of over 3% in the penumbra region, the penumbra was steeper and so the maximum distance to agreement was below 3mm. The same levels of agreement were seen for 10MV as for 6MV.

The agreement between the calculated and measured horizontal profiles for the obliquely incident fields was excellent. In the high dose gradient regions, all isodoses corresponded to within 2mm and in the low dose gradient parts of the curves, all calculated doses agreed with measurement to within 2% and usually to within 1% at both profile depths.

The repeatability of the relative dose measurements in the study of the effect of missing back- and side-scatter was better than 0.2% (1 standard deviation). The algorithm underestimated the effect of the missing side-scatter, generally overestimating the doses. However, for all fields studied, only when the measurement point was within 1.5cm of the lateral extent of the phantom did any significant difference between measured and predicted doses of greater than 2% occur. The mean discrepancy at 1.5cm from the edge was 1.4% ± 0.3%; at 2.0cm, the mean value was 1.0% ± 0.3% and at 3cm 0.3% ± 0.2%. The largest dose error was in the presence of just 1 cm of side scatter for the 10x10cm field, where the AAA overestimated the dose by 4.0% at both energies. The effect of missing backscatter was not predicted at all by the AAA, the calculated depth doses towards the bottom of the phantom being identical to those at the same depths in the presence of full backscatter. This resulted

in an overestimate of the dose at a point 1cm from the back of the phantom of up to 1.5% for a 10x10cm field and up to 2.5% for a 20x20cm field compared to the measured values. The overestimate was larger for larger fields and was greater for a 6MV beam than a 10MV beam.

Inhomogeneous Geometries

The results of the point dose measurements beneath the various inhomogeneity layers are summarised in Table 2. Measurements made in a homogeneous Plastic Water[TM] phantom using the same set-up showed agreement with calculation to within 0.3%. In the presence of inhomogeneities, all the point dose measurements agreed with calculation to within 2.5%. The agreement between calculated and measured doses under bone equivalent material was better at 10MV than at 6MV.

As can be seen in Figure 4, the AAA predicts the broadening of the beam penumbra in a low density medium well; maximum discrepancies for this relatively shallow depth of cork were 2.5% or 2.5mm, apart from in the heel of the curve.

The depth dose curve measured in the Plastic Water[TM] and Styrofoam phantom, shown in Figure 5, demonstrated that while the PBC algorithm does not model the reduction in dose in the low density medium, the AAA does predict the reduction and re-build-up. Discrepancies of up to 2% between the measured and calculated percentage depth doses in the Styrofoam and between 2% and 3% beyond the Styrofoam were seen. However, with an estimated overall uncertainty of approximately 2.5% on these measurements using the Farmer chamber in Styrofoam, these discrepancies can not be considered significant.

Two of the simulated treatment plans on the CIRS phantoms are shown in Figure 6. A summary of the differences between calculated and measured doses in these plans is given in Table 3, with corresponding results for the PBC model shown for comparison.

It can be seen that for the AAA all measurement points show agreement to within 2.5% except for two points in the 3-field plan – the point near the field edge is in the high dose gradient and the distance to agreement is less than 1mm, while the spinal cord point is in a low dose region and has a distance to agreement of 1.7mm. The AAA consistently provides better agreement with measurement than the PBC model, particularly within the lung regions. While the distance to agreement for the field edge

point in the 3-field plan was 1mm for the PBC plan, all other points for which the dose discrepancy exceeded 2.5% had associated distances to agreement of between 2.4mm and 11mm.

Discussion

Many recommendations for acceptable levels of accuracy in treatment planning systems have been published (for example, [9,11,27,28]). The specific parameters to be tested and their associated tolerances vary between these publications, but consensus would appear to be moving towards requiring agreement to between 2 – 3% in low dose gradient regions and 2 – 3mm in high dose gradients. In the UK, the guidelines in IPEM Report 81 [11] suggest an "ideal" agreement as being to within 2% or 2 mm of the beam normalisation value and an "acceptable" level for the same regions are 3% and 3mm respectively. Van Dyk [27] specified further limits for more complex situations – 3% for simple beams with inhomogeneity and 4% or 4mm for more complex situations with inhomogeneities (but 3% in low dose gradient regions). In this work, profiles and depth doses were compared at 0.25mm intervals.

The measurements entered into the planning system during configuration of the AAA are PDD curves and profiles at five depths for a range of field sizes from 40x40cm down to at least 4x4cm. The simple, unwedged geometries tested demonstrated that the iterative adjustment of the generic beam intensity profiles performed during configuration produced unit-specific beams that matched the measured data at the "ideal" level. The dose distributions for even the most elongated fields – of clinical relevance in, for example, craniospinal treatments – were accurately calculated. Similarly successfully prediction of MLC fields, which additionally incorporate the modified phase space modelling of the AAA, was achieved.

Larger discrepancies were seen with the Enhanced Dynamic Wedge fields. The largest errors were measured at the high dose end of the wedge; this might be expected given that the final separation of the jaws during such a treatment is just 0.5cm – somewhat smaller than the smallest field size entered in the configuration. The poorer performance for EDW fields agree with those reported by Fogliata *et al.* [8], who also found a wedge angle dependence of the wedge factor (calculated as a wedge "transmission factor" in that report). The accuracy of the AAA in the specific case of small fields is of

particular importance not only for EDW fields but for IMRT dose calculations and is the topic of continuing investigation at Weston Park Hospital.

The algorithm was found to predict the effect of missing side scatter well, especially in the more clinically relevant areas. The only significant difference in the case of the oblique fields was the high dose gradient region of the vertical depth dose of the 20° incidence field. This was a result of the relatively shallow angle at which the plane of the depth dose crossed the penumbra of the angled field, but for the 10 x 10 field studied, this occurred at a depth of approximately 20cm and was in a relatively low dose region. The profile and depth doses closer to the surface all showed excellent agreement. Similarly, the largest discrepancies for the tangential fields occurred in the 1cm closest to the surface. Such a situation is clearly of most relevance for glancing beams used in treatments of the breast and chest wall. The overestimate of the dose in the most superficial area must be borne in mind when evaluating such plans, but the magnitude of the differences are smaller than those of the underestimates of the Pencil Beam Convolution model with ETAR correction.

The limitations of pencil beam algorithms in treatments involving low density inhomogeneities are well documented [2,5,6,7,15,20,29]. In this study, the AAA has been shown to account for the increase in lateral electron transport in terms of the broadening of the penumbra in low density material and predicting the reduction in central axis dose in such a low density heterogeneity. It was found to slightly underestimate this dose reduction in the Styrofoam, but this material represents an extreme situation, having a density significantly lower than that found in the lung [14]. In the more clinically realistic situation of the simulated treatment plans, good agreement between the AAA and measurement was seen in the lung regions (whose relative electron density was approximately 0.2). The model did not appear to predict a build-down region immediately above the Styrofoam, which is consistent with the failure to predict the effect of the lack of backscatter, but more detailed measurements close to the interface are required to determine the magnitude of this effect.

The point dose measurements below the slabs of inhomogeneity give a general feeling for the ability of the algorithm to predict the dose in the presence of laterally extended heterogeneities. It would appear that at both energies, the algorithm overestimates the dose beyond the cork inhomogeneity (as would be expected from the depth doses with the Styrofoam block), where it does not beyond the air gap. The algorithm appeared to overestimate the effect of the bone slab. However, few conclusions

can be drawn from these limited measurements and further work investigating the effects of inhomogeneities, particularly interface effects close to the boundaries between them, is ongoing.

The simulated treatment plans delivered to the thorax phantom allow some measure of the overall performance of the algorithm to be gained. The first plan comprised three fields, all with MLC and two with EDW and oblique incidence, the second two wedged fields, also with MLC. The different geometries clearly involved passing through different combinations of lung, water-equivalent tissue and bone. In both cases, the point dose measurements agreed with the AAA's predictions to within 2.5% or 2mm, indicating that in the clinical situation, the algorithm appears to perform to the desired level of accuracy.

One further aspect that is of importance in the clinical situation is the speed with which an algorithm performs the required dose calculations. Comparisons of calculation time using the PBC and AAA models with inhomogeneity correction were favourable. For example, a 3-field lung plan calculated on a 120-slice dataset at 2.5mm calculation grid spacing took 265 seconds using our currently implemented algorithm, the PBC with ETAR inhomogeneity correction, while the AAA took just 75 seconds.

The AAA is just one of many convolution-superposition models implemented in commercial treatment planning systems; the collapsed cone convolution (CCC) models of the Pinnacle [16,21] and Helax-TMS [1] planning systems (ADAC, Milpitas, CA, USA and Nucletron, Veenendaal, Netherlands respectively) are perhaps the most widely studied in the literature. The accuracy of these two algorithms has been evaluated in several studies; while exact comparison of the results in those reports with the results obtained in this study is not practical, some general comments can be made. Performance in homogeneous conditions was reported at the same level – generally to within 2% or 2mm – for the three algorithms [3,10,18]. The AAA, in common with the Pinnacle CCC model, performed slightly better than the Helax CCC model within low density inhomogeneities, but slightly worse beyond them [19]. Similar levels of accuracy in predicting the effect of missing side-scatter were seen with the AAA and Helax CCC model, although the latter model predicts the effect of missing backscatter while the AAA does not [3,18]. The AAA gave slightly better agreement with measurement in the simulated treatment plans compared to similar investigations involving the Helax CCC model. The accuracy of the AAA is dependent upon the quality of the initial modelling of the beams in Eclipse;

agreement between calculation and measurement may vary between centres according to how well the beams are modelled.

Conclusions

In this study we have investigated the accuracy of dose calculations performed with the Anisotropic Analytical Algorithm in a range of situations from single fields in homogeneous media to full simulated treatment plans applied to semi-anthropomorphic phantoms.

Modelling of homogeneous phantom situations was found to be generally correct to within 2% or 2mm agreement, with no systematic differences between 6MV and 10MV. Calculations in the presence of inhomogeneities also showed good agreement. Measurements made of the doses in the semi-anthropomorphic phantom from the simulated treatment plans indicate the overall performance in the presence of complex fields, missing tissue geometries and inhomogeneous media. These showed very good agreement with calculation, all points agreeing to within 2.5% or 2mm. The accuracy of the AAA represents an improvement over the currently implemented Pencil Beam Convolution model, particularly in the presence of low density inhomogeneities and compares well with other commercially available convolution superposition algorithms.

References

[1]   Ahnesjö A and Aspradakis MM. Dose calculations for external photon beams in radiotherapy. Phys. Med. Biol.1999;44**:**R99-R155

[2]   Arnfield MR, Siantar CH, Siebers J, Garmon P, Cox L and Mohan R. The impact of electron transport on the accuracy of computed dose. Med. Phys. 2000;27:1266-1274

[3]   Aspradakis MM, Morrison RH, Richmond ND and Steele A. Experimental verification of convolution ∕ superposition photon dose calculations for radiotherapy treatment planning. Phys. Med. Biol. 2003;48:2873-2893

[4]   Brahme A, Chavaudra J, Landberg T *et al.* Accuracy requirements and quality assurance of external beam therapy with photons and electrons. Acta Oncologica 1988;27:S1-S76 (Suppl. 1)

[5]   Carrasco P, Jornet N, Duch MA *et al.* Comparison of Dose Calculation Algorithms in Phantoms With Lung Equivalent Heterogeneities Under Conditions of Lateral Electronic Disequilibrium. Med. Phys. 2004;31:2899-2911

[6]   De Jaeger K, Hoogeman MS, Engelsman M *et al.* Incorporating an Improved Dose-Calculation Algorithm in Conformal Radiotherapy of Lung Cancer: Re-Evaluation of Dose in Normal Lung Tissue. Radiother. Oncol. 2003;69:1-10

[7]   Engelsman M, Damen EMF, Koken PW, van't Veld AA, van Ingen, KM, Mijnheer, BJ. Impact of simple tissue inhomogeneity correction algorithms on conformal radiotherapy of lung tumours. Radiother. Oncol. 2001;60:299-309

[8]   Fogliata A, Nicolini G, Vanetti E, Clivio A and Cozzi L. Dosimetric validation of the anisotropic analytical algorithm for photon dose calculation: fundamental characterization in water. Phys. Med. Biol. 2005;51:1421-1438

[9]   Fraass B, Doppke K, Hunt M *et al.* American Association of Physicists in Medicine Radiation Therapy Committee Task Group 53: Quality Assurance for clinical radiotherapy planning. Med. Phys. 1998;25:1773-1829

[10]   Gifford KA, Followill DS, Liu HH and Starkschall G. Verification of the accuracy of a photon dose-calculation algorithm. J. Appl. Clin. Med. Phys. 2002;3:26-45

[11]   Institute of Physics and Engineering in Medicine (IPEM) Report 81. Physics aspects of quality assurance in radiotherapy. York: IPEM; 1999

[12] International Commission on Radiological Units (ICRU) Report 24. Determination of absorbed dose in a patient irradiated by beams of X or gamma rays in radiotherapy procedures. Washington DC: ICRU; 1976

[13] International Commission on Radiological Units (ICRU) Report 42. Use of computers in external beam radiotherapy procedures with high-energy photons and electrons. Bethseda MD: ICRU; 1987

[14] International Commission on Radiological Units (ICRU) Report 44. Tissue substitutes in radiation dosimetry and measurement. Bethseda, MD: ICRU; 1989

[15] Koelbl O, Krieger K, Haedinger U, Sauer O and Flentje M. Influence of calculation algorithm on dose distribution in irradiation of non-small cell lung cancer (Nsclc) - Collapsed Cone versus Pencil Beam. Strahlenther. Onkol. 2004;180:783-788

[16] Mackie TR, Bielajew AF, Rogers DWO and Battista JJ. Generation of photon energy deposition kernels using the EGS Monte Carlo code. Phys. Med. Biol. 1988;33:1-20

[17] Mijnheer BJ, Battermann JJ and Wambersie A. What degree of accuracy is required and can be achieved in photon and neutron therapy? Radiother. Oncol. 1987;8:237–252

[18] Nisbet A, Beange I, Vollmar H-S, Irvine C, Morgan A and Thwaites DI. Dosimetric verification of a commercial collapsed cone algorithm in simulated clinical situations. Radiother. Oncol. 2004;73:79-88

[19] Paelinck L, Raynaert N, Thierens H, De Neve W and De Wagter C. Experimental verification of lung dose with radiochromic film: comparison with Monte Carlo simulations and commercially available treatment planning systems. Phys. Med. Biol. 2005;50:2055-2069

[20] Papanikolaou N, Battista J, Boyer A *et al.* Tissue inhomogeneity corrections for megavoltage photon beams. AAPM Report No 85 Task Group 65 of the Radiation Therapy Committee of the American Association of Physicists in Medicine. Madison, WI: Medical Physics Publishing; 2004

[21] Papanikolaou N, Mackie TR, Meger-Wells C, Gehring M and Reckwerdt P. Investigation of the convolution method for polyenergetic spectra. Med. Phys. 1993;20:1327-1336

[22] Shahine BH, Al-Ghazi MSAL, El-Khatib E. Experimental evaluation of interface doses in the presence of air cavities compared with treatment planning algorithms. Med. Phys. 1999;26:350-355

[23] Storchi PRM, van Battum LJ and Woudstra E. Calculation of pencil beam kernel from measured photon beam data. Phys. Med. Biol. 1999;44:2917-2928

[24] Ulmer W and Harder, D. Applications of a triple Gaussian pencil beam model for photon beam treatment planning. Z. Med. Phys. 1996;3:68-74

[25] Ulmer W and Kaissl W. A triple Gaussian pencil beam model for photon beam treatment planning. Z. Med. Phys. 1995;5:25-30

[26] Ulmer W, Pyyry J and Kaissl W. A 3D photon superposition/convolution algorithm and its foundation on results of Monte Carlo calculations. Phys. Med. Biol. 2005; 50:1767-1790

[27] van Dyk J, Barnett RB, Cygler JE and Shragge PC. Commissioning and quality assurance of treatment planning systems. Int. J. Radiat. Oncol. Biol. Phys. 1993;26:261-273

[28] Venselaar JLM, Welleweerd J and Mijnheer BJ. Tolerances for photon beam dose calculations using a treatment planning system. Radiother. Oncol. 2001;60:191-201

[29] Wang L, Yorke E and Chui CS. Monte Carlo Evaluation of 6 MV intensity modulated radiotherapy plans for head and neck and lung treatments. Med. Phys. 2002;29:2705-2717

Figures

Figure 1   Set-ups for the evaluation of (a) missing backscatter and (b) missing side-scatter
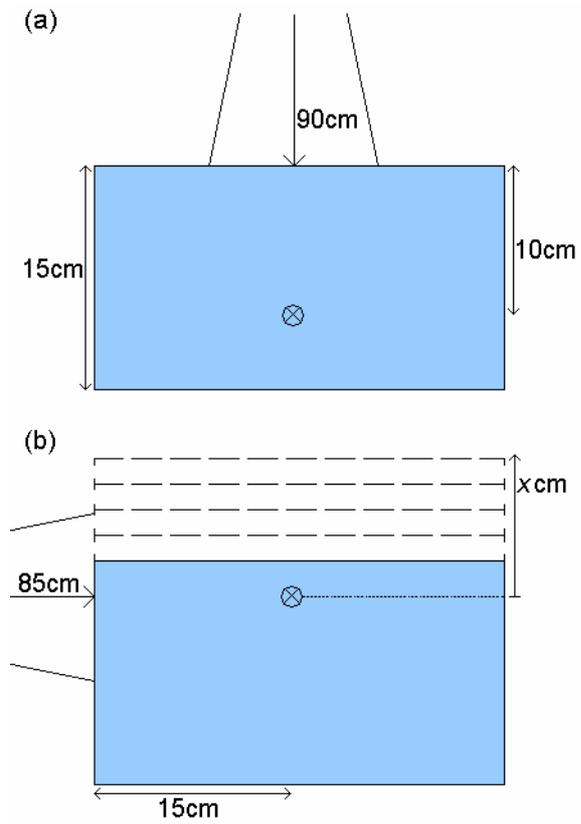
Figure 2 60° symmetric measured (circles) and calculated (dotted line) EDW profiles and 60° half-

beam blocked measured (crosses) and calculated (solid line) EDW profiles. (The wedged

field profiles have been reversed for clarity.) All doses are normalised to the measured

central axis dose for the 60º symmetric EDW field.
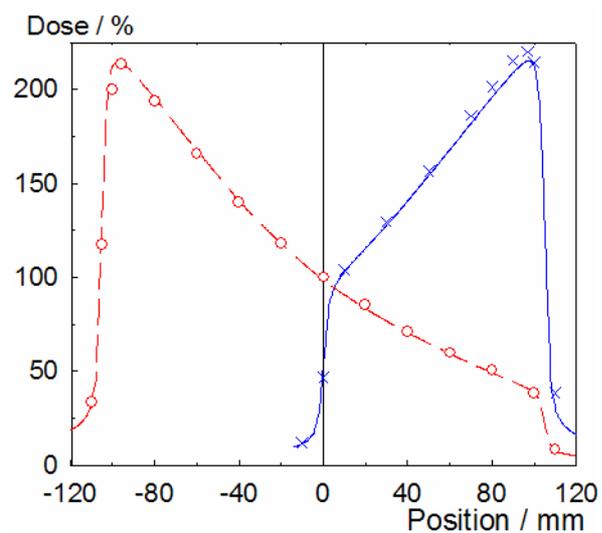
Figure 3   Calculated (solid lines) and measured (dashed lines) depth dose curves, measured in the

vertical plane, for the fields incident at 0°, 20° and 30° to the vertical.
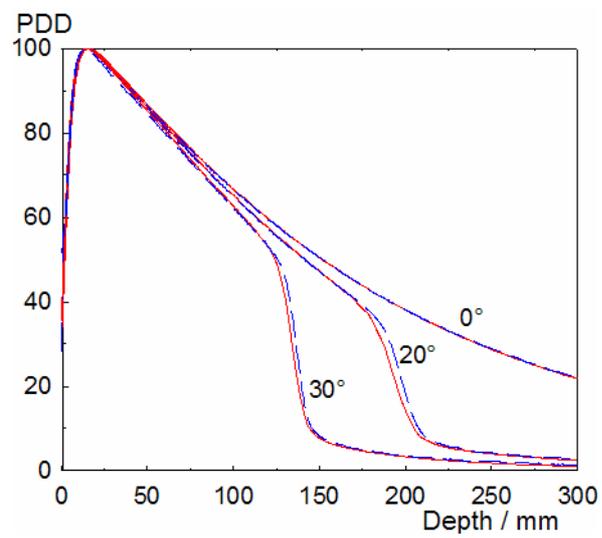
Figure 4 Measured (solid lines) and calculated (crosses) profiles within a block of cork. The dotted line indicates the calculated profile in water at the same depth, for comparison. The dose values are normalised to the central axis dose of the profile in water.
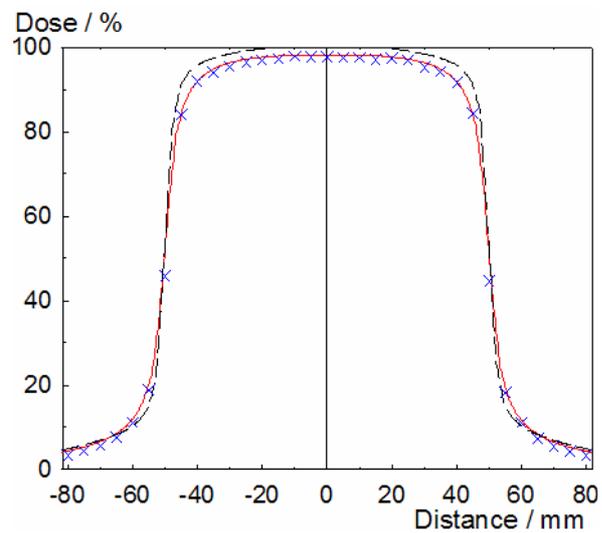
Figure 5   Depth doses measured in the Plastic Water^{TM} and Styrofoam phantom (crosses) and the curves calculated with the PBC model (dotted line) and AAA (solid line).
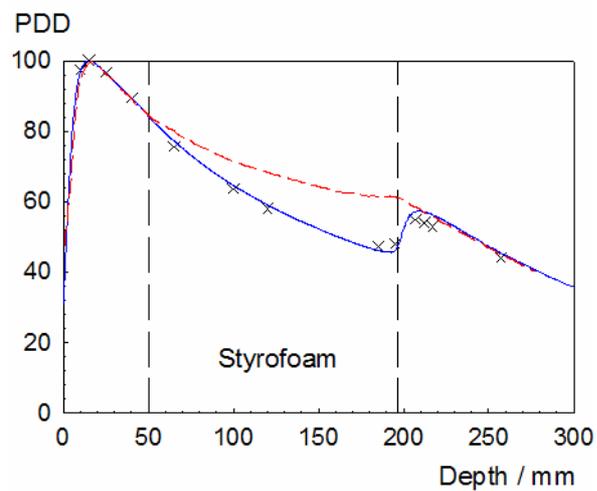
Figure 6   Treatment plans on the CIRS thorax phantom showing the points of measurement.
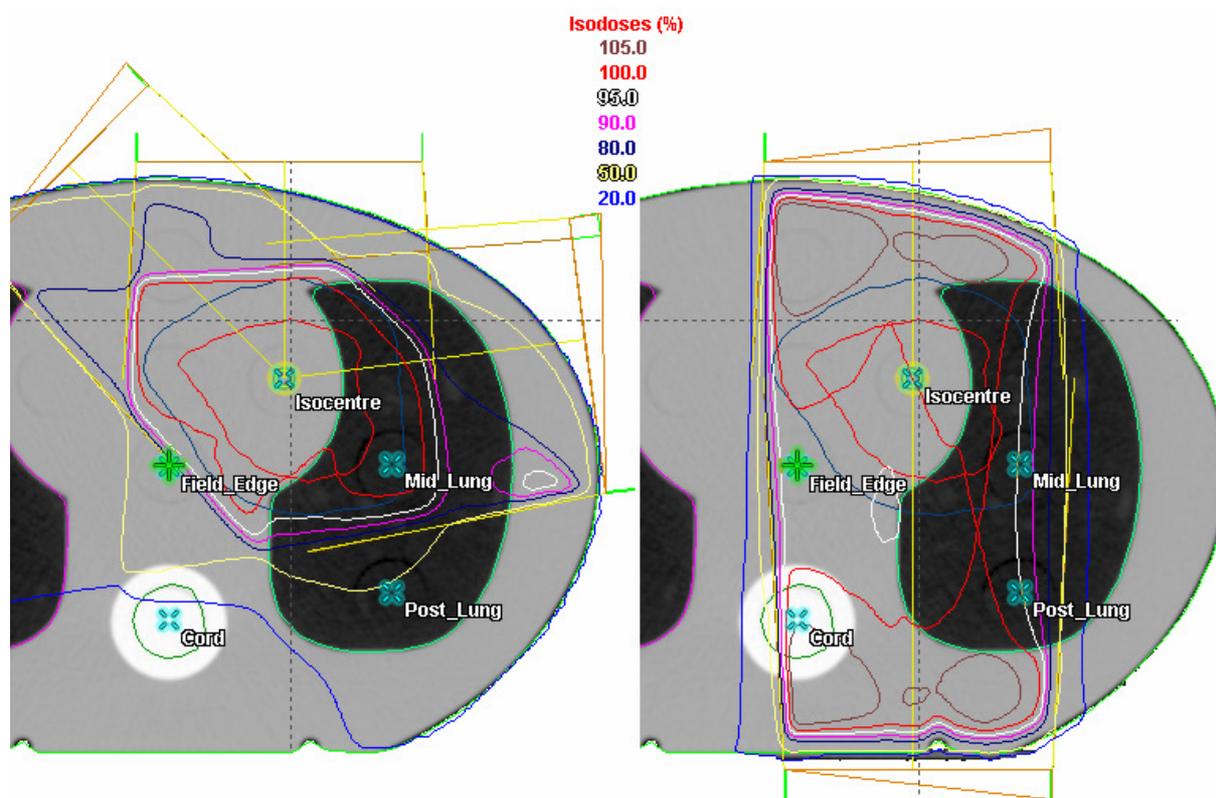
Table 1 Summary of the experimental set-ups for simple, complex and slab phantom geometries

	Description	Measurements	Field Details	SSD
Simple geometries				
S1	Square fields	PDD, Profiles	4x4cm to 40x40cm	100cm
S2	Rectangular fields	PDD, Profiles	4x15cm, 15x4cm, 5x20cm, 20x5cm, 5x30cm, 30x5cm, 5x40cm, 40x5cm	100cm
S3	MLC-defined fields	PDD, Profiles	4x4cm, 10x10cm, 20x20cm fields; jaws 2cm beyond MLC leaves	100cm
S4	Different SSD	PDD, Profiles	4x4cm, 10x10cm, 15x15cm, 20x20cm	90cm, 120cm
S5	EDW fields	WF, Profiles	10x10cm, 20x20cm Wedge factors for 15, 30, 45, 60° EDW Profiles for 30, 60° EDW	100cm
Complex geometries				
C1	Asymmetric fields	PDD, Profiles	Half-beam block: (5,5)x(0,5), (10,10)x(0,10) Jaw over axis: (10,10)x(-2,10)	100cm
C2	Asymmetric fields	Profiles	60° EDW fields, (5,5)x(0,5), (10,10)x(0,10)	100cm
C3	Oblique incidence	PDD, Profiles	10x10cm, GA = 20°, 30° Profiles at d=2.5cm and d=7.5cm	97.5cm
C4	Missing scatter	Point doses	4x4cm, 10x10cm, 15x15cm, 20x20cm	90/85cm
C5	Tangential fields	Point doses	5x5cm, 15x15cm	85cm
Inhomogeneous slabs				
I1	Slab phantom	Point doses	2cm Plastic Water^{TM} –5cm air–3cm Plastic Water^{TM} – chamber – 10cm Plastic Water^{TM}	90cm
I2	Slab phantom	Point doses	2cm Plastic Water^{TM} –5cm cork–3cm Plastic Water^{TM} – chamber – 10cm Plastic Water^{TM}	90cm
I3	Slab phantom	Point doses	3cm Plastic Water^{TM} –2cm solid bone–5cm Plastic Water^{TM} – chamber – 10cm Plastic Water^{TM}	90cm
I4	Slab phantom	Point doses	7cm Plastic Water^{TM} –2cm solid bone–1cm Plastic Water^{TM} – chamber – 10cm Plastic Water^{TM}	90cm
I5	Slab phantom	Point doses	2cm Plastic Water^{TM} –2cm solid bone–4cm cork– 2cm Plastic Water^{TM} – chamber – 10cm Plastic Water^{TM}	90cm
I6	Slab phantom	Profiles	7cm Plastic Water^{TM} –3cm cork–Film–2cm cork– 13cm Plastic Water^{TM}	100cm
I7	Low density	PDD	5cm Plastic Water^{TM} –14.7cm Styrofoam–10cm Plastic Water^{TM}	100cm

Table 2   Differences between calculated and measured point doses (%) at 10 cm depth

Geometry	6MV	10MV
I1	+0.9	+1.0
I2	+2.4	+2.3
I3	-1.3	-0.1
I4	-1.4	-0.1
I5	+2.1	+1.9

Table 3   Differences between calculated and measured doses (%) for the simulated treatment plans in the CIRS thorax phantom using the Anisotropic Analytical Algorithm and Pencil Beam Convolution models.

Reference Point	AAA	PBC
3-field plan		
Isocentre	+0.5	+0.6
Mid Lung	-0.8	+4.7
Posterior Lung	-2.1	+2.4
Spinal Cord	-2.7	+3.7
Outside PTV (field edge)	+4.0	+4.4
Parallel Pair		
Isocentre	-1.2	-2.2
Mid Lung	+1.3	+7.5
Posterior Lung	+1.5	+7.4
Spinal Cord	-0.8	-1.8
Outside PTV (field edge)	-0.8	+0.5

Acknowledgements